



# Phage-Enhanced Materials: Antimicrobial Films and Coatings Targeting *Pseudomonas fluorescens* and *Escherichia coli*

Fernanda Coelho<sup>1,2</sup> · Victor Gomes Lauriano de Souza<sup>2,3</sup> · Lorenzo Pastrana<sup>2</sup> · Sanna Sillankorva<sup>2</sup> · Valtencir Zucolotto<sup>1</sup>

Received: 14 May 2025 / Accepted: 5 August 2025 / Published online: 23 August 2025  
© The Author(s), under exclusive licence to Springer Science+Business Media, LLC, part of Springer Nature 2025

## Abstract

The development of scalable and efficient antimicrobial food packaging solutions is critical for food safety, especially in addressing pathogenic bacterial contamination. This study highlights the use of ultrasonic spray coating (USC) technology, which provides a high-yield, scalable, and roll-to-roll compatible method for producing coatings with consistent quality and minimal material waste. Bacteriophages were explored as antimicrobial agents in food packaging due to their specificity and ability to remain active over time when embedded in biopolymer matrices, which can support a gradual and sustained antimicrobial effect. A phage cocktail targeting *Escherichia coli* and *Pseudomonas fluorescens* was incorporated into sodium alginate-based solutions to create antimicrobial films and coatings. Phage FSB24, targeting *P. fluorescens*, belongs to the *Studiervirinae* subfamily and *Pifdecavirus* genus, while phage North, targeting *E. coli*, is part of the *Straboviridae* family and *Krischvirus* genus. Phage-infused sodium alginate solutions were processed into cast films and coatings on paper and polystyrene substrates using USC technology. The materials were evaluated for phage load, physical properties (thickness, moisture content, water vapor permeability, swelling index), chemical interactions (FTIR), surface morphology (SEM), and antimicrobial activity. The results showed that phage inclusion did not alter the physical properties compared to control samples. Phage FSB24 demonstrated superior antimicrobial performance against *P. fluorescens*, while phage North was effective against *E. coli*. This study demonstrates the potential of sodium alginate-based films and coatings containing bacteriophages, produced by USC technology, as effective, scalable solutions for antimicrobial food packaging, enhancing food safety and preventing bacterial contamination.

**Keywords** Antimicrobial packaging · Ultrasonic spray coating · Food safety · Phage cocktail

## Introduction

The rapid growth of the food industry has made food safety and quality assurance essential priorities, requiring the development of more efficient and scalable packaging solutions. Bacterial contamination continues to be a major challenge in the food supply chain, resulting in significant economic losses due to spoilage and health risks to consumers (Costa et al., 2023). Food processing is a critical stage in this chain, as factors such as inadequate temperature control, cross-contamination, and lack of equipment sanitization contribute to the spread of bacteria. This contamination can alter the texture, flavor, color, and nutritional value of food, compromising its quality and safety, as well as causing food-borne diseases, affecting millions globally each year (World Health Organization, 2024).

✉ Fernanda Coelho  
fernanda.coelho1408@gmail.com

✉ Sanna Sillankorva  
sanna.sillankorva@inl.int

<sup>1</sup> Nanomedicine and Nanotoxicology Group (Gnano), São Carlos Institute of Physics, University of São Paulo, São Carlos, São Paulo, Brazil  
<sup>2</sup> International Iberian Nanotechnology Laboratory, Braga, Portugal  
<sup>3</sup> Departamento de Química, MEtRICs/CubicB, NOVA School of Science and Technology, FCT NOVA, Universidade Nova de Lisboa, Campus de Caparica, 2829-516 Caparica, Portugal

Growing concerns about infectious contamination have led to the development of packaging solutions that reduce the risk of pathogens and extend the shelf life of food (Anvar et al., 2021). In this context, active packaging materials (APM) have emerged as an innovative solution, with enhanced properties such as mechanical strength, thermal stability, gas exchange, and notably, antimicrobial activity against foodborne pathogens (Pandey et al., 2022).

Bacteriophages — viruses that specifically target bacteria — are particularly useful in controlling pathogens during food storage and processing (Costa et al., 2023). They offer several advantages as natural antimicrobials in the food industry, including high specificity, effectiveness at low doses, food safety, ease of isolation, and cost-effective propagation. Furthermore, they help extend the shelf life of food and preserve its organoleptic qualities, such as texture, flavor, color, and aroma (Costa et al., 2023).

To make this method scalable, ultrasonic spray coating (USC) technology addresses these challenges by providing up to 95% transfer efficiency, minimal waste, and the ability to create thin and uniform films, unlike conventional coating methods such as air spraying, which face limitations in transfer efficiency and material waste. By combining an ultrasonic atomizer with controlled devices, USC offers precise control over the coating process, making it ideal for scalable production, especially in roll-to-roll systems (Feng et al., 2023).

Recent research on phage delivery systems has shown promising results in preventing bacterial colonization and maintaining phage activity over time, with the potential for controlled release. The selection of biomaterials for these systems should be tailored to the needs of each food application, considering factors such as food type, biomaterial properties, and phage compatibility (Gonzalez-Menendez et al., 2018). For example, phage-loaded coatings have been successfully applied to cheese, poultry, and fresh-cut produce to inhibit pathogens like *Listeria monocytogenes*, *Escherichia coli*, and *Salmonella enterica*, demonstrating real-world potential for controlling spoilage and ensuring food safety (Viazis et al., 2011; Soni et al., 2016; García-Anaya et al., 2023).

These approaches facilitate the development of scalable structures and enable efficient phage retention, with options for controlled and targeted release (Yang et al., 2023). In this study, a phage cocktail was incorporated into a sodium alginate solution, and films and coated substrates (parchment paper and polystyrene) were prepared using ultrasonic coating. These materials were characterized and evaluated for their physicochemical, mechanical, and antimicrobial properties, with the aim of proposing a new optimized delivery system for food packaging.

## Materials and Methods

### Materials

Alginate sodium salt, magnesium nitrate, and sodium chloride were acquired from Sigma-Aldrich (Portugal). Glycerol 99.5% (v/v) was purchased from Alfa Aesar (USA), Tris base and Poly(ethylene glycol) (PEG)8000 were purchased from Fisher BioReagents™ (USA), and calcium chloride and MgSO<sub>4</sub> from Panreac Applichem (Spain).

### Bacteria

In this study, *Pseudomonas fluorescens* ATCC 27663 and *Escherichia coli* BL21 (Invitrogen, ThermoFisher Scientific) were used as hosts for phage isolation. These bacteria were grown at 37 °C in liquid or solid TSB medium (TSB + 1.5% (w/v) of agar).

## Phage Isolation and Characterization

### Phage Isolation

Phages were isolated from raw sewage collected from a wastewater treatment plant in Frossos, Braga, Portugal (collected June 2024), following an enrichment procedure. Briefly, the sewage samples were first centrifuged at 9000 × g for 15 min to remove debris before proceeding with phage isolation. Equal volumes of the centrifuged sewage and double-strength LB were combined in an Erlenmeyer flask and inoculated with 50 µL of an overnight culture of the target bacteria. The mixture was then incubated for 24 h at 120 rpm, under the optimal growth conditions for each bacterium: 37 °C for *E. coli* and 30 °C for *P. fluorescens*. After incubation, the samples were centrifuged again (9000 × g, 4 °C, 15 min), and the supernatants were filtered through a 0.22 µm polyether sulfone (PES) syringe filter. These enriched samples were then spotted onto bacterial lawns of the respective hosts using the double-agar overlay technique (1). Plates were incubated overnight at the optimal growth temperature for each bacterial host. The presence of inhibition zones on the bacterial lawns indicated the potential presence of phages in the enriched samples. Since the inhibition zones may result from multiple phages, further isolation was performed by picking and re-plating a single phage plaque at least three times or until a consistent plaque morphology was achieved (2). The diameter of 5 phage plaques was determined using ImageJ software (version 1.54g).

## Phage Propagation and Titration

The plate lysis and elution method previously described was used for phage propagation. This procedure is adapted from the methodology described by Sambrook and Russell (2001) but has some modifications. Phage titration was performed as described by Adams (1959).

## Phage Growth Parameters

One-step growth curves of phage in its host strains were performed, as previously described by Pajunen et al. (2000). Briefly, 10 mL of mid-exponential phase host bacterium were centrifuged ( $7000\times g$ , 10 min), the pellet was resuspended (5 mL of fresh TSB) and adjusted to an OD<sub>600</sub> (UV-1600PC Spectrophotometer) of 0.6 (*P. fluorescens*) and 0.4 (*E. coli*). After, 5 mL of the respective phage was added to have a final multiplicity of infection (MOI) of 0.001. Phages were allowed to adsorb for 5 min at 37 °C, and after the sample was centrifuged (9000 rpm, 5 min). The pellet was resuspended in 10 mL of fresh TSB and incubated at 37 °C. Samples were taken periodically for 60 min and immediately plated for PFU enumeration.

## Transmission Electron Microscopy (TEM)

Phages FSB24 and North were centrifuged for 1 h ( $25,000\times g$ , 4 °C). The pellet was washed once in tap water, and 1 mL of MilliQ water was added. The sample was again centrifuged (1 h,  $25,000\times g$ , 4 °C), and the pellet was resuspended in 50  $\mu$ L of MilliQ water. After, phages were deposited on copper grids (400 mesh), stained with 2% (w/v) uranyl acetate (pH 4.0), and imaged at 200 kV using a JEM-2100-HT electron microscope (JEOL, Tokyo, Japan).

## Phage Genome Sequencing, Annotation, and Comparative Genomics

Phage DNA was extracted following the instructions of the Quick-DNA™ Viral Kit (D3015, Zymo Research) and the concentration was measured on Nanodrop. The quality control of the sample was analyzed by Nanodrop by evaluation of the 260/280 and 260/230 ratios, and by electrophoresis (100 V, 3 h) using a 1% (w/v) agarose gel. The library construction was carried out using the KAPA HyperPlus kit. The generated DNA fragments (DNA libraries) were sequenced in the Illumina MiSeq, using 300 bp paired-end sequencing reads, and the quality control of raw data generated was performed. Contigs were assembled with BV-BRC (<https://www.bv-brc.org/app/Assembly2>), using Unicycler (auto) and SPAdes as assembly strategy, and sorting assemblies by ARAST quality score and manual inspection. The genome sequence was drawn using

Proksee (Grant et al., 2023). Comparative analysis of the entire genome with reference sequences was performed with BLASTn (<https://blast.ncbi.nlm.nih.gov/>). Whole-genome comparisons using Progressive MAUVE were performed (Darling, et al., 2010). Pairwise comparisons of the nucleotide sequences were performed using the Genome-BLAST Distance Phylogeny (GBDP) 3.0 under the recommended settings for prokaryotic viruses (Meier-Kolthoff et al., 2013; Meier-Kolthoff & Goker, 2017) and phylogeny was inferred using the Virus Classification and Tree Building Online Resource (VICTOR) (Meier-Kolthoff, J.P. & Goker, M, 2017). Intergenomic distances were utilized to infer a balanced minimum evolution tree, with branch support calculated using FASTME. Subtree Pruning and Regrafting (SPR) postprocessing was applied to optimize the tree based on the D0 formula. Branch support was assessed using 100 pseudobootstrap replicates (Lefort et al., 2015).

## Fabrication of Antimicrobial Films by Casting and Coatings on Paper and Plastic Substrates by Ultrasonic Coating

### Preparation of Antimicrobial Solution

A 1% (w/v) sodium alginate solution was prepared in distilled water under continuous stirring at room temperature for 18 h. Afterward, glycerol was added at a concentration of 0.5% (v/v) and the solution was stirred at 250 rpm. Phages FSB24 and North were then incorporated to achieve a final concentration of approximately  $10^7$  PFU/mL in the films and coatings, followed by stirring for 30 min at room temperature.

### Antimicrobial Film Fabrication by Casting

To produce the films, 20 mL of the film-forming solution (FFS) was cast onto a 9.2 cm diameter Petri dish and dried at 30 °C for 24 h. Cross-linking of the films with a CaCl<sub>2</sub> solution supplemented with phages at a concentration of approximately  $10^8$  PFU/mL was performed using the “immersion film” method (Alves et al., 2019). In this method, the dried films in Petri dishes were soaked for 5 min in a 0.2% (w/v) CaCl<sub>2</sub> solution. After immersion, the excess CaCl<sub>2</sub> solution was discarded, and the films were dried again at 30 °C for 24 h. A sodium alginate solution without phages was also prepared as a control.

### Antimicrobial Paper and Plastic Substrates Production Using Ultrasonic Coating

The FFS was coated onto two substrates (parchment paper and polystyrene) using an Ultrasonic Spray Coater (Versa-Coat, SonoTek, USA) equipped with a Propel Nozzle (120

Hz). Coatings were applied using a flow rate of 0.5 mL/min, run power of 2.0 W at a speed of 50 mm/s, onto the defined area in 10 layers. Coated substrates were left to dry naturally at room temperature inside the equipment's chamber with an exhausting system to speed up the drying process. One single layer of 0.2% CaCl<sub>2</sub> (w/v) was applied using the same conditions used for the FFS, aiming at the crosslinking of sodium alginate. Substrates coated with the FFS free of the phage cocktail were also prepared, and paper or polystyrene without coating were defined as control samples. Figure 1 shows the ultrasonic coating process applied to the paper and polystyrene substrates.

## Characterization of Antimicrobial Films and Coatings

### Thickness, Grammage, and COBB Test

The thickness of the substrates was measured at five different points for each sample using a digital micrometer (Schut, BN Groningen, The Netherlands) with an accuracy of  $\pm 0.001$  mm. The grammage of the uncoated (control) and coated substrates was determined according to the ASTM D646-96 methodology (American Society for Testing and Materials [ASTM], 2007). The samples were weighed on a semi-analytical balance (ARD110, Ohaus Corporation, Morris, NJ, USA) and the grammage was calculated according to Eq.

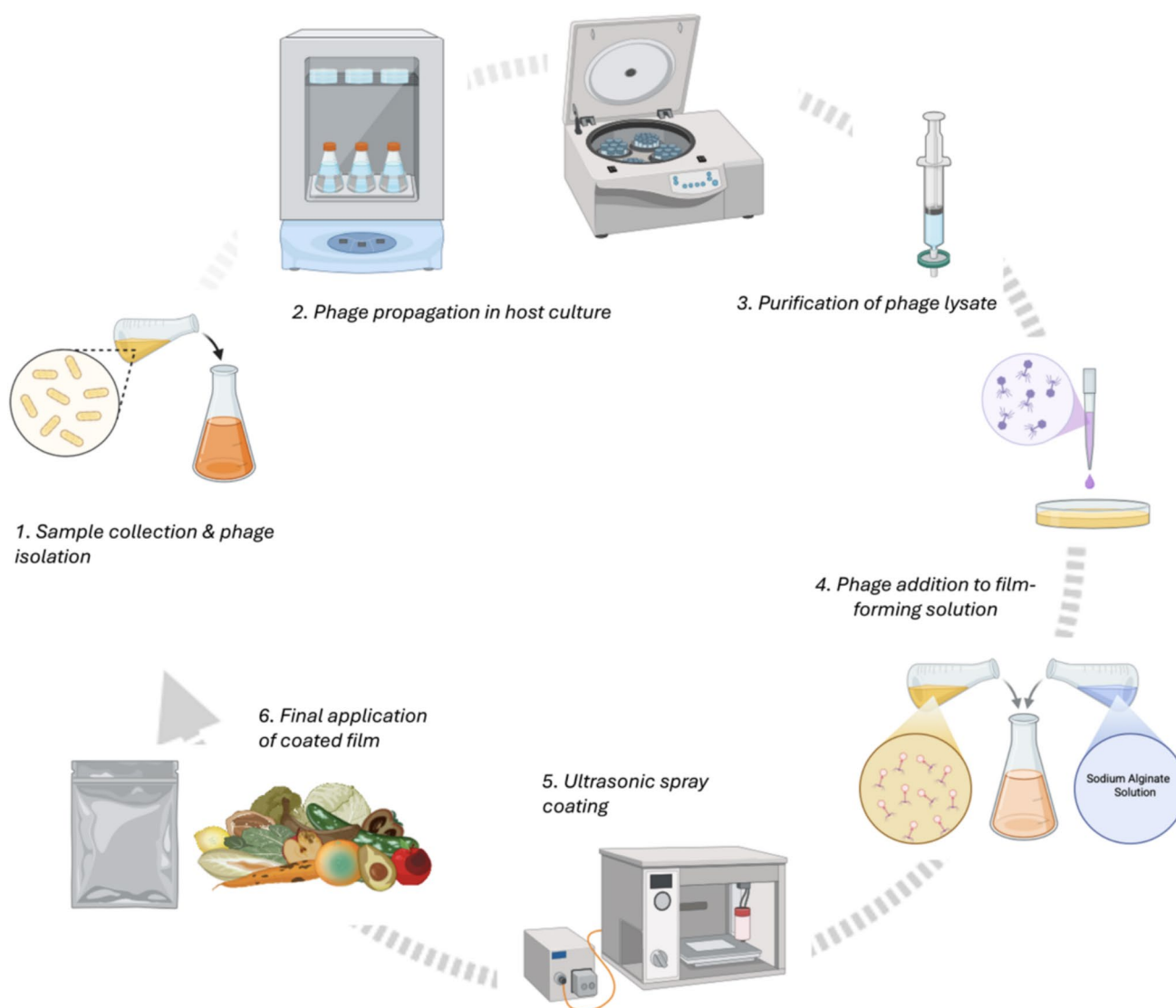


**Fig. 1** Schematic representation of the process from bacteriophage recovery to film preparation. The steps include phage isolation, propagation in bacterial cultures, purification, incorporation into a film-

forming solution, and application via ultrasonic spray coating. The ultrasonic spray coating step is emphasized as a key innovation in this process

(1), where  $G$  = grammage ( $\text{g}/\text{m}^2$ );  $M$  = mass of the paper (g);  $A$  = area ( $\text{m}^2$ ).

$$G = \frac{M}{A} \quad (1)$$

The water absorption capacity ( $\text{WAC}_{\text{Cobb}}$ ) of paper samples was evaluated according to Tappi 441 om-98 (2004). Briefly, pre-weighted samples with  $12.5 \times 12.5$  cm were placed in the Cobb testing apparatus (Techlabsystems, Spain) and water (100 mL) was poured onto the samples, confined by the equipment ring. After 60 s, the water was removed, and to eliminate the excess water, the samples were placed between two sheets of absorbent paper (blotting paper) and quickly pressed with a 10 kg cylindrical stainless steel roller (rolling it twice over the protected sample). Afterward, the samples were weighed using a semi-analytical balance (ARD110, Ohaus Corporation, Morris, NJ, USA).  $\text{WAC}_{\text{Cobb}}$  was calculated according to Eq. (2).

$$\text{WAC}_{\text{Cobb}} = \frac{(M_f - M_i)}{0.01} \quad (2)$$

### Opacity and Color

Opacity was determined according to the Hunter Lab method, as the ratio between the opacity of each sample on a black standard ( $Y_b$ ) and the opacity of each sample on a white standard ( $Y_w$ ) (Eq. 3). Measurements were taken three times for each film sample and substrate.

$$\text{Opacity} = \left( \frac{Y_b}{Y_w} \right) \times 100 \quad (3)$$

The color of the samples was assessed using a Cielab colorimeter (model PCECSM7). The  $L^*$ ,  $a^*$ , and  $b^*$  values of each film were obtained through reflectance measurements. In this system,  $L^*$  represents lightness (ranging from black to white), while the horizontal axes, indicated by  $a^*$  and  $b^*$ , represent chromatic coordinates (from  $-a^*$ : green and  $-b^*$ : blue to  $+a^*$ : red and  $+b^*$ : yellow). The chroma  $C^*$  (Eq. 4) and the hue angle  $h^\circ$  (Eq. 5) are the polar coordinates considering a cylindrical model. The values of  $a^*$  and  $b^*$  approach zero for neutral colors and increase as the color becomes more saturated and chromatic.

$$C^* = \left( \frac{a^{*2}}{b^{*2}} \right) \times 0.5 \quad (4)$$

$$h^\circ = \text{atan} \left( \frac{b^*}{a^*} \right) \quad (5)$$

### Scanning Electron Microscopy (SEM)

The surface and thickness morphology of the films and coatings were examined using SEM (Quanta FEG 650, FEI, USA). The samples were gold-coated (Leica EM ACE200), and an accelerating voltage of 10 kV was applied at various magnifications to capture the images.

### Swelling

The swelling (SW) of the films was determined following a modified version of the method described by Alves et al. (2019). Films were cut into  $2 \times 2$   $\text{cm}^2$ , and their initial weight was recorded. The pre-weighted films were then immersed in distilled water for 24 h at room temperature. After immersion, excess water was gently removed using filter paper, and the films were weighed again. The percentage of absorbed water was calculated using Eq. (6), where  $S_1$  represents the weight of the film after immersion and  $S_0$  is the film's initial weight. All measurements were conducted in triplicate for each film type.

$$\text{SW}(\%) = \frac{(S_1 - S_0)}{S_0} \times 100 \quad (6)$$

### Surface Hydrophobicity and Water Vapor Permeability (WVP)

Surface hydrophobicity was determined as described by Espitia et al. (2014). In brief, sodium alginate films and coatings, both with and without phages, were evaluated for hydrophobicity by measuring the contact angle 60 s after a water droplet made contact with the sample surface, using the sessile drop method. The contact angle was measured using a contact angle goniometer (OCA 20, DataPhysics, Germany), where a 5  $\mu\text{L}$  droplet of ultrapure water was placed on the sample surface with a precision syringe (500  $\mu\text{L}$ , Hamilton, Switzerland). The Laplace-Young equation was applied to calculate and fit the droplet profile. At least three independent measurements were taken for each sample.

Water vapor permeability (WVP) was measured following the desiccant method ASTM E96/E96M (American Society for Testing and Materials [ASTM], 2013). The samples were sealed onto a 35 mm diameter Payne 5100 permeability cup (Elcometer SPRL, Hermelle/s Argenteau, Belgium) containing 10 g of  $\text{CaCl}_2$  (0% Relative Humidity – 0%RH) and placed inside a desiccator with super saturated magnesium nitrate solution (54% RH, 20 °C). To ensure uniform conditions for all samples, a fan was used inside the desiccator. The cups were weighed periodically to monitor weight gain over time until a steady state was reached. The water vapor transmission

rate (WVTR) was then calculated by dividing the slope of the linear regression of weight gain over time by the surface area of the film. WVP ( $\text{g m}^{-1} \text{s}^{-1} \text{Pa}^{-1}$ ) was calculated using Eq. (7), where  $L$  represents the film thickness (m), and  $\Delta P$  is the partial vapor pressure difference (Pa) between the two sides of the sample. For each measurement, at least three replicates were performed for each sample.

$$WVP = \frac{(WVTRXL)}{\Delta P} \quad (7)$$

### Mechanical Properties

The tensile strength (TS), elongation at break (EB), and Young's Modulus (YM) of the samples were assessed using a Universal Testing Machine (AGX-V 10 kN, Shimadzu, Japan), equipped with a 500N load cell. The measurements followed the methodology outlined in ASTM D882–10 (American Society for Testing and Materials [ASTM], 2010), with some modifications, and an initial gauge length of 4 cm. The calculations for TS and EB were based on Eqs. (8) and (9), respectively. YM was determined from the slope of the initial linear portion of the stress–strain curves. Samples measuring 50 mm × 20 mm were secured between grips with an initial distance of 40 mm. Force and deformation data were recorded during stretching at a rate of 50 mm/min. The results for TS and EB were reported in MPa and percentage, respectively. Each sample was tested in at least six replicates.

$$TSB(\text{MPa}) = \frac{\text{maximum load (N)}}{\text{initial cross-sectional area (m}^2\text{)}} \quad (8)$$

$$EB(\%) = \frac{\text{final length at the point of sample rupture (mm)}}{\text{Initial length of the specimen (mm)}} \quad (9)$$

### Fourier Transform Infrared Spectroscopy (FTIR)

FTIR spectra of the samples were obtained using a Bruker Alpha II FTIR spectrometer (Bruker FT-IR VERTEX 80/80v, Boston, USA), operating within a wavelength range of 500 to 4000  $\text{cm}^{-1}$  at a resolution of 4  $\text{cm}^{-1}$ , employing the Platinum Attenuated Total Reflection (ATR) mode (Bruker, Germany). The absorbance values for each FTIR spectrum were normalized to a range between 0 and 1.

### Phage Stability and Antimicrobial Efficacy

#### Phage Stability

The stability of *E. coli* and *P. fluorescens* bacteriophages was evaluated over a 15-day period under different environmental

conditions. Phage suspensions, as well as phage-coated films, parchment paper, and polystyrene substrates, were exposed to a range of temperatures and pH values to simulate stress conditions. The materials were incubated in contact with buffered solutions of varying pH and maintained at different temperatures for up to 15 days. At defined time intervals, samples were collected and the phage viability was assessed by determining the plaque-forming units (PFUs). All assays were performed in triplicate.

#### Loading Efficiency

The loading efficiency and release of phages in sodium alginate films and coatings were evaluated using PFU/mL measurements. For *E. coli*, the theoretical loading was determined to be  $9.8 \times 10^7$  PFU/mL for films and  $5.9 \times 10^7$  PFU/mL for coatings. For *P. fluorescens*, the theoretical loading was  $1.5 \times 10^8$  PFU/mL for films and  $9.0 \times 10^7$  PFU/mL for coatings.

#### Coating Stability

The stability of coating samples on parchment paper and plastic using a sodium alginate solution mixed with phages was evaluated over a 15-day period. The samples were stored at room temperature throughout the study. To ensure reliability and reproducibility, all experiments were conducted in triplicate.

#### Antimicrobial Activity

The antimicrobial activity of phage-coated substrates and films was evaluated according to the ISO 22196 standard. Phage-coated and control samples were prepared using *E. coli* and *P. fluorescens* as test organisms. Bacterial cultures were adjusted to approximately  $10^5$  CFU/mL, and 100  $\mu\text{L}$  of each suspension was uniformly spread onto the surface of the samples. The inoculated samples were then covered with a sterile polyethylene film to ensure even contact and incubated for 24 h at 37 °C for *E. coli* and 30 °C for *P. fluorescens*. After incubation, bacteria were recovered by rinsing the sample surfaces with a neutralizing solution, followed by serial dilution. Surviving bacterial counts were determined by plating on selective agar: CHROMagar™ ECC for *E. coli* and Plate Count Agar (PCA) for *P. fluorescens*. Antimicrobial efficacy was expressed as log reduction in CFU compared to the control samples. All experiments were performed in triplicate.

#### Statistical Analysis

Statistical analysis was conducted using the analysis of variance (ANOVA) method, and Tukey's test for mean

comparison was performed using Statistica software for Windows (version 12, StatSoft Inc., Tulsa, OK, USA). A *p*-value of less than 0.05 was deemed statistically significant.

## Results and Discussion

### Bacteriophage Characteristics

Two bacteriophages were isolated and characterized in this study. Phage FSB24 was obtained using *Pseudomonas fluorescens* ATCC 27663 as host. It produced clear plaques with an average diameter of  $3.4 \pm 0.6$  mm (Fig. 2a), suggesting a lytic lifestyle. Transmission electron microscopy (TEM) analysis revealed a podovirus-like morphology, with a short non-contractile tail ( $10.8 \pm 2.3$  nm in diameter,  $12.4 \pm 0.6$  nm in length) and an icosahedral capsid of  $57.5 \pm 1.9$  nm in diameter (Fig. 2b). This structure is consistent with phages belonging to the Autographiviridae family.

The one-step growth curve (Fig. 2c) showed a latent period of approximately 15 min and a remarkably short burst period of 10 min. The burst size was calculated to be  $142.2 \pm 39.1$  PFU per infected cell, indicating efficient viral

replication and host lysis. Notably, two replication cycles occurred within the 60-min experiment, reinforcing the potential of FSB24 as a fast-acting biocontrol agent.

Genomic analysis revealed a linear double-stranded DNA genome of 39,145 bp with a GC content of 58%, aligning with values reported for related *Pseudomonas* phages. A total of 58 coding sequences (CDSs) were predicted, of which 37 encode hypothetical proteins, three are conserved phage proteins, and 18 have known or predicted functions (Fig. 2d). Functional annotation allowed the organization of genes into modules associated with DNA replication, packaging, structural components, lysis, and host interaction (Table S1). Despite the high proportion of hypothetical proteins, the presence of key genes such as DNA polymerase, capsid proteins, and holin-endolysin systems supports its classification within the Studiervirinae subfamily.

Phylogenetic analysis using VICTOR placed FSB24 among members of the Pifdecavirus genus, showing close relationships with phages UNO-SLW3, UNO-SLW4, UNO-SL2, and UNO-SLW1 (Fig. 2e). This placement was supported by progressive MAUVE alignment, which revealed high genome synteny and sequence similarity among these phages (Figure S1). Interestingly, phages within this clade infect a range of *Pseudomonas* species, and some, such as

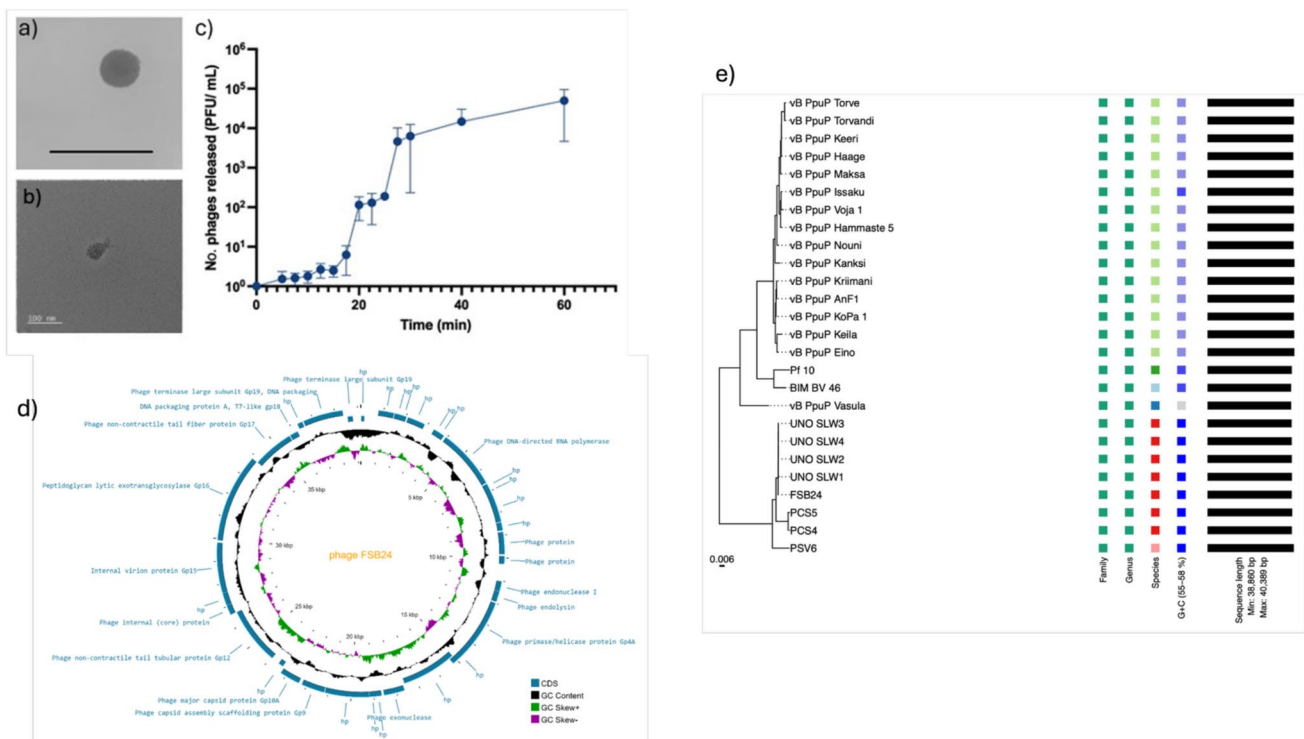


**Fig. 2** *Pseudomonas* phage FSB24 features. **a** Plaque morphology (scale bar=1 cm). **b** Virion morphology observed using TEM (scale bar=100 nm). **c** One-step growth curve. **d** Genome map of *Pseudomonas* phage FSB24 showing predicted coding sequences (CDSs)

and their functions, GC content, and GC skew (+/−). “hp” indicates hypothetical proteins. Visualization created using Proksee. **e** Midpoint-rooted phylogenetic tree of *Pseudomonas* phage FSB24 and the 25 most homologous phages identified via BLAST

vB\_PfIP-PCS4 and vB\_PfIP-PCS5, are known for their broad host range, including *P. putida*, *P. alcaligenes*, *P. tolaasii*, and *P. fragi* (Johno et al., 2024). These features underscore the potential applicability of FSB24 in biocontrol strategies targeting multiple *Pseudomonas* spp.

Moreover, GC content analysis revealed a pattern among related phages: those clustering below FSB24 in the phylogenetic tree (e.g., vB\_PfIP-PCS5) tend to exhibit higher GC content, whereas the vB\_PupP# phages infecting *P. putida* have comparatively lower GC values. This observation may reflect host-specific genomic adaptations and could serve as an additional criterion for taxonomic resolution within this group.

Phage North was isolated using a clinical *Escherichia coli* strain recovered from a urinary tract infection. This strain displayed multidrug resistance, including resistance to amoxicillin–clavulanic acid, AmpC  $\beta$ -lactamases, cefuroxime, ciprofloxacin, and colistin (Table S2), highlighting its clinical relevance and the urgent need for alternative treatments. Phage North also demonstrated the ability to infect the laboratory strain *E. coli* BL21, which was subsequently used for phage propagation and characterization due to its safety and tractability.

Phage North produced small, clear plaques with a diameter of  $0.78 \pm 0.01$  mm, indicative of efficient host lysis and lytic behavior (Fig. 3a). TEM imaging revealed

a contractile-tailed virion, characteristic of the Myoviridae morphotype. The virion comprises a capsid measuring  $53.5 \pm 4.0$  nm in diameter and a tail  $120.7 \pm 4.3$  nm in length and  $17.3 \pm 1.7$  nm in diameter (Fig. 3b). These structural features are consistent with phages of the Straboviridae family and Krischvirus genus.

The one-step growth experiment revealed a latent period of approximately 10 min and a single replication cycle within the 60-min observation window (Fig. 3c). The burst size was determined to be  $60.5 \pm 4.1$  PFU per infected bacterium, which, while lower than that observed for phage FSB24, still supports effective amplification and suggests potential as a therapeutic agent against resistant *E. coli* strains.

Whole-genome sequencing revealed a large genome of 164,180 bp with a GC content of 40.46%, aligning with the genomic characteristics of other Krischvirus phages. The genome harbors 300 predicted coding sequences (CDSs), including 45 hypothetical proteins, 150 putative phage proteins, and 105 genes with assigned functions (Fig. 3d). Functional annotation allowed the grouping of these genes into replication, structural, packaging, and lysis modules, analogous to the functional architecture described for phage FSB24 (Table S2). The large genome size of phage North is at the upper limit for members of Krischvirus, possibly reflecting its broader functional and adaptive capacity.

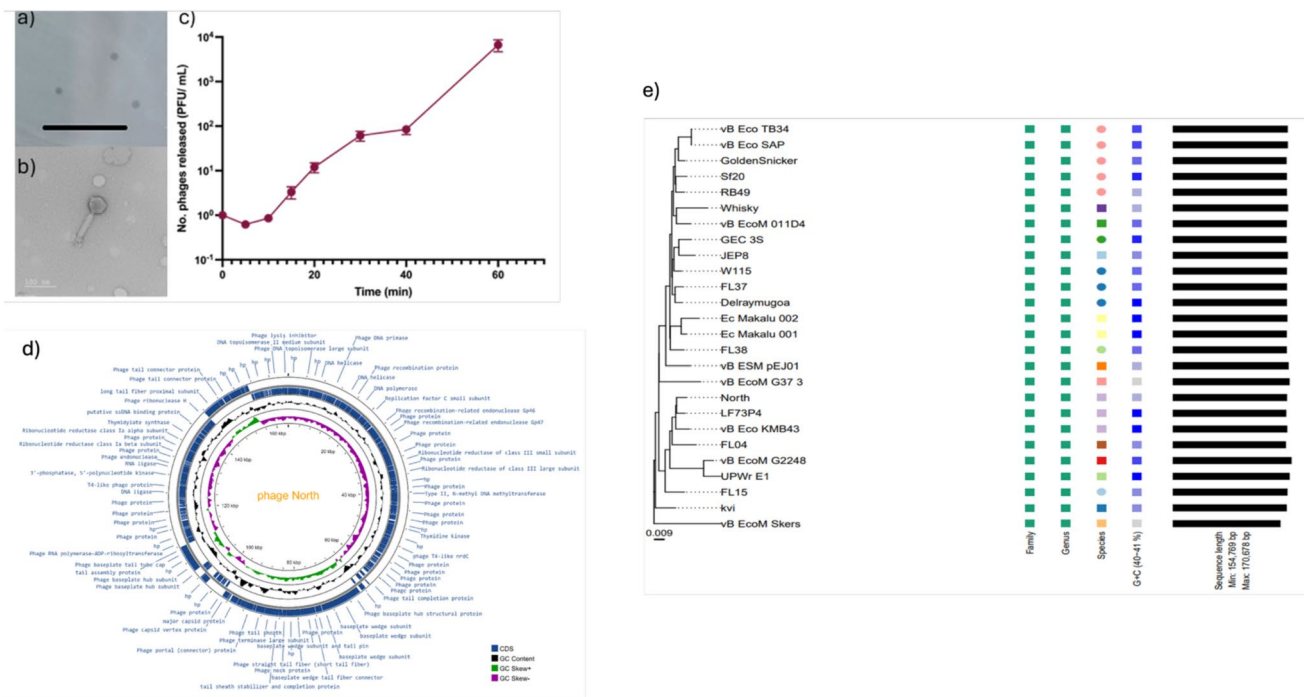


**Fig. 3** *Escherichia* phage North features. **a** Plaque morphology (scale bar=1 cm). **b** Virion morphology observed using TEM (scale bar=100 nm). **c** One-step growth curve. **d** Genome map of *Escherichia* phage North showing predicted coding sequences (CDSs) and

their functions, GC content, and GC skew (+/–). “hp” indicates hypothetical proteins. Visualization created using Proksee. **e** Mid-point-rooted phylogenetic tree of *Escherichia* phage North and the 25 most homologous phages identified via BLAST

Comparative genomic analysis using progressive MAUVE revealed more than ten locally collinear blocks (LCBs) among related phages, contrasting with the largely conserved genome structure of phage FSB24 (Figure S2). This suggests higher genomic plasticity and extensive rearrangements among Krischvirus members, which may be associated with adaptation to diverse *E. coli* hosts.

Phylogenetic reconstruction (Fig. 3e) showed that phage North clusters closely with LF73P4, forming a tight clade within the broader Krischvirus lineage. This clade is further associated with phages vB\_EcoM\_KMB43 and FL04, which likely represent the same species based on genetic similarity and branch support. All phages in this cluster share similar genome lengths and GC content (40–41%), reinforcing their taxonomic proximity.

Altogether, the structural, genomic, and phylogenetic characteristics of phage North support its classification within Straboviridae/Krischvirus and its potential use in phage therapy, particularly against multidrug-resistant *E. coli* strains.

### Thickness, Grammage, and COBB Test

To endure the mechanical demands of handling, storage, and transportation, food packaging materials need adequate strength and flexibility to support the weight of the food. The film thickness ranged from 30  $\mu\text{m}$  to 34  $\mu\text{m}$ , meeting the standard definition for a film (less than 0.25 mm) (Wang et al., 2020). As indicated in Table 1, the coatings slightly increased the substrates' thickness, corroborated by grammage measurements, and suggesting successful polymer deposition.

Similar increases in thickness and grammage in substrates coated with natural polymers have been noted in the literature. For instance, Tanpichai et al. (2022) developed paper

coated with one to five chitosan layers, observing a consistent rise in thickness and weight with each additional layer. Initially, the uncoated paper measured 74.5  $\mu\text{m}$  in thickness and weighed 44.65  $\text{g}/\text{m}^2$ . With one layer of chitosan, thickness increased by about 28%, and weight by around 5%.

The Cobb values for alginate-coated samples were marginally higher than for uncoated samples, however, with no statistical significance ( $p > 0.05$ ). From these measurements, in line with findings by Kopacic et al. (2018), we conclude that alginate coating enhances the hydrophilicity of the samples, regardless of the substrate.

### Opacity and Color

Opacity is a key optical property for food packaging materials, as it directly influences the protection of the product against light-induced oxidative degradation (Alves et al., 2024). Increased opacity can contribute to extending shelf life by limiting the exposure of food to UV and visible light (Petraru & Amariei, 2023).

As shown in Table 1, the Chroma values of the coated samples did not differ significantly from the control ( $p > 0.05$ ), indicating that the sodium alginate coating did not alter the saturation or intensity of the color. This suggests that the coating maintains the visual neutrality of the material, which is important for consumer acceptance and product visibility when transparency is desired.

Interestingly, the opacity results revealed a slight increase in opacity for parchment paper substrates after coating, while a minor decrease was observed for polystyrene. This contrast may be attributed to the interaction of the alginate solution with the surface properties and porosity of each substrate. The increased opacity in parchment paper might result from partial absorption and film formation within its fibrous matrix, whereas the smoother

**Table 1** Thickness, grammage, water absorption (COBB test), chroma, hue ( $^{\circ}$ ), opacity ( $\text{mm}^{-1}$ ), contact angle ( $^{\circ}$ ), and water vapor transmission rate (WVTR,  $\text{g}/\text{m}^2\cdot\text{day}$ ) values for the different material matrices

Matrix		Thickness ( $\mu\text{m}$ )	Grammage ( $\text{g}/\text{m}^2$ )	COBB Test ( $\text{g}/\text{m}^2$ )	Chroma	Hue ( $^{\circ}$ )	Opacity ( $\text{mm}^{-1}$ )	Contact angle ( $^{\circ}$ )	WVTR ( $\text{g}/\text{m}^2\cdot\text{day}$ )
Parch- ment paper	Control	40.17 $\pm$ 2.59 <sup>B</sup>	—	11.73 $\pm$ 0.02 <sup>A</sup>	1.47 $\pm$ 0.03 <sup>B</sup>	73.22 $\pm$ 0.05 <sup>A</sup>	32.48 $\pm$ 1.55 <sup>A</sup>	107.55 $\pm$ 7.85 <sup>A</sup>	233.31 $\pm$ 4.46 <sup>A</sup>
	Without phages	51 $\pm$ 1.41 <sup>A</sup>	3.90 $\pm$ 0.04 <sup>A</sup>	13.82 $\pm$ 0.42 <sup>A</sup>	1.60 $\pm$ 0.02 <sup>AB</sup>	75.92 $\pm$ 0.67 <sup>B</sup>	33.97 $\pm$ 0.33 <sup>A</sup>	83.15 $\pm$ 3.89 <sup>B</sup>	202.16 $\pm$ 1.24 <sup>A</sup>
	With phages	51.83 $\pm$ 3.06 <sup>A</sup>	3.82 $\pm$ 0.17 <sup>A</sup>	13.05 $\pm$ 1.27 <sup>A</sup>	1.72 $\pm$ 0.09 <sup>A</sup>	77.92 $\pm$ 0.63 <sup>B</sup>	36.49 $\pm$ 0.58 <sup>A</sup>	95.15 $\pm$ 0.78 <sup>AB</sup>	199.31 $\pm$ 18.32 <sup>A</sup>
Polysty- rene	Control	57.67 $\pm$ 2.36 <sup>B</sup>	—	0.14 $\pm$ 0.03 <sup>A</sup>	1.08 $\pm$ 0.03 <sup>B</sup>	75.32 $\pm$ 0.02 <sup>A</sup>	16.84 $\pm$ 0.31 <sup>A</sup>	91.45 $\pm$ 0.21 <sup>A</sup>	15.32 $\pm$ 0.87 <sup>A</sup>
	Without phages	68.33 $\pm$ 1.18 <sup>A</sup>	2.78 $\pm$ 0.07 <sup>A</sup>	0.65 $\pm$ 0.33 <sup>A</sup>	1.26 $\pm$ 0.00 <sup>A</sup>	80.39 $\pm$ 1.27 <sup>AB</sup>	15.86 $\pm$ 0.01 <sup>B</sup>	66 $\pm$ 3.81 <sup>B</sup>	14.59 $\pm$ 1.09 <sup>A</sup>
	With phages	69.83 $\pm$ 1.18 <sup>A</sup>	2.89 $\pm$ 0.13 <sup>A</sup>	0.23 $\pm$ 0.42 <sup>A</sup>	1.16 $\pm$ 0.05 <sup>AB</sup>	79.11 $\pm$ 1.66 <sup>B</sup>	15.96 $\pm$ 0.15 <sup>B</sup>	73.05 $\pm$ 0.1 <sup>B</sup>	14.88 $\pm$ 0.54 <sup>A</sup>
Na-alg- inate Film	Without phages	30.83 $\pm$ 2.12 <sup>A</sup>	—	—	2.60 $\pm$ 0.45 <sup>A</sup>	85.11 $\pm$ 0.52 <sup>A</sup>	13.21 $\pm$ 0.45 <sup>A</sup>	52.70 $\pm$ 2.54 <sup>A</sup>	637 $\pm$ 17.28 <sup>A</sup>
	With phages	33.83 $\pm$ 9.19 <sup>A</sup>	—	—	1.86 $\pm$ 0.79 <sup>A</sup>	83.52 $\pm$ 1.45 <sup>A</sup>	13.39 $\pm$ 0.23 <sup>A</sup>	48.55 $\pm$ 5.16 <sup>A</sup>	602.66 $\pm$ 13.67 <sup>A</sup>

surface of polystyrene could lead to a thinner, more uniform coating that slightly reduces light scattering.

Hue values remained stable across all samples, suggesting that the coating did not alter the perceived color tone of the materials. This reinforces the finding that the sodium alginate solution did not induce any noticeable color shift.

Figure 4 presents representative digital images of both the control and coated materials, visually confirming the minimal impact of the coating on the overall appearance. The coatings were visually uniform and did not introduce opacity or coloration that would interfere with the aesthetic qualities of the substrates.

Overall, the data suggest that sodium alginate coatings preserve the optical properties of packaging materials, which is advantageous for applications where both visual presentation and light barrier properties are important.

## Scanning Electron Microscopy (SEM)

The surface morphology and cross-section of the samples were examined using a high-vacuum scanning electron microscope (Quanta FEG 650, FEI, USA), operated at an accelerating voltage of 15 kV. The images showed that the control samples were coated with sodium alginate solution, and the sodium alginate solution films displayed a uniform surface. Figure 5 illustrates these SEM images of the sample surfaces and cross-sections.

The surface of the coated materials exhibited a slightly porous structure, which may be attributed to the intrinsic characteristics of the alginate network and the drying process. This observation is consistent with the findings of Jost et al. (2014), who reported that such porosity can result from the partial evaporation of water molecules initially bound to the alginate matrix. As water evaporates during drying, it may leave behind microvoids within the polymer structure, contributing to the formation of a porous network. This

**Fig. 4** The figure shows digital images of the control materials and those coated with sodium alginate solution. **A** Polystyrene substrate — control. **B** Polystyrene substrate coated with sodium alginate solution. **C** Film of sodium alginate solution. **D** Parchment paper — control. **E** Parchment paper coated with sodium alginate solution

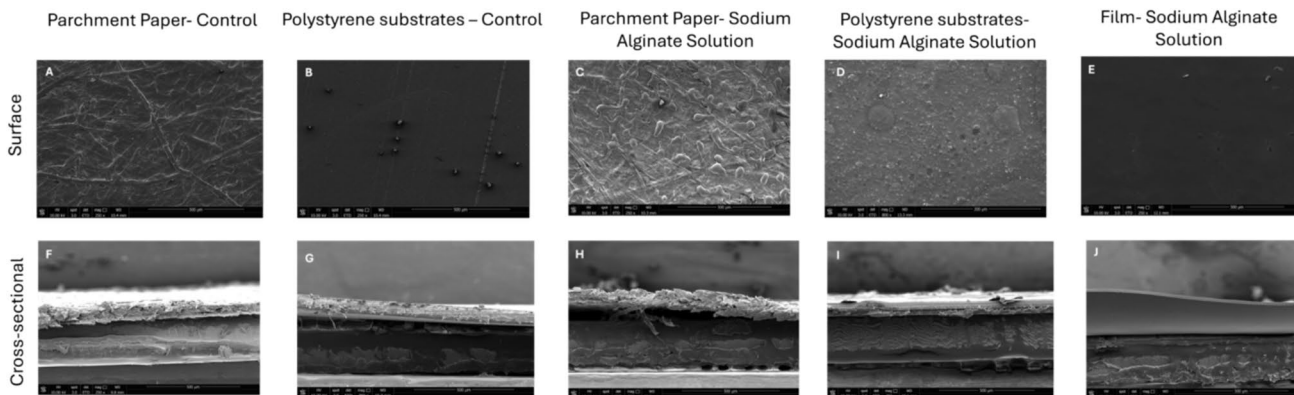


**Fig. 5** SEM images. 250 X of the surface and cross-sectional views

structural feature could influence not only the barrier properties of the coating but also its mechanical behavior and interaction with external agents, depending on the degree and distribution of porosity.

### Swelling of the Alginate Films

Alginate-based films are promising candidates for the development of edible films for food applications. These films provide uniform, transparent barriers with effective oxygen permeability, though their hydrophilic nature leads to low water resistance. Alginates can interact with di- and trivalent cations, particularly calcium ions. Recent studies have shown that crosslinking alginate-based films with calcium ions improves tensile strength, thereby enhancing structural cohesion and producing stronger films with reduced water solubility (Costa et al., 2018). In this study, films crosslinked with only 0.2% (w/v) of  $\text{CaCl}_2$  demonstrated complete solubility, making it impossible to measure the swelling index. However, this characteristic is advantageous for refrigerated food applications, where contact with moisture can facilitate rapid phage release, achieving an optimal concentration for antimicrobial effectiveness.

### Surface Hydrophobicity and Water Vapor Permeability (WVP)

To assess the samples' moisture interaction after coating, water contact angles were measured. As shown in Table 1, the uncoated parchment paper (control) exhibited a high contact angle of  $107.55^\circ$ , attributed to its natural roughness. Coated paper samples, with or without phages, demonstrated reduced contact angles. A similar trend was observed in polystyrene substrates, where coating resulted in lower contact angles. This is likely due to the hydrophilic nature of sodium alginate, allowing droplets to spread more easily across the surface. Additionally, the low contact angles seen in alginate films confirm the polymer's hydrophilic characteristics.

Effective water vapor and gas barrier properties are crucial for packaging materials. Tests on uncoated paper and plastic samples served as controls under defined conditions. The high-water vapor transmission rate (WVTR) observed in uncoated paper samples is likely linked to the porous

structure of the material, as indicated by SEM characterization (see the “[Scanning Electron Microscopy \(SEM\)](#)” section). The hydrophilic cellulose fibers in paper readily absorb moisture, resulting in elevated WVTR values (Li et al., 2007). However, a modest reduction in WVTR was observed after sodium alginate coating on parchment paper and polystyrene, probably due to the extra physical barrier created by the coating.

Sodium alginate films, regardless of phage presence, showed high WVTR values. This result is attributed to sodium alginate's hydrophilicity, which can lead to increased water absorption and, consequently, higher WVTR as more water vapor permeates the material. Furthermore, alginate films may retain environmental moisture, further contributing to elevated WVTR values as they equilibrate with surrounding conditions.

Superscript letters (A-B): Within each respective material group, values in the same column not sharing upper case superscript letters indicate statistically significant differences between each other ( $p < 0.05$ ).

### Mechanical Properties

The mechanical properties of the control materials, including tensile strength (TS) and elongation at break (EB), remained largely unaffected by the addition of the sodium alginate coating (Table 2). However, a decrease in Young's modulus (YM) was observed in the coated parchment paper. This reduction aligns with alginate's hydrophilic properties, as it can absorb water and soften in humid environments, thus enhancing the material's elasticity (Parreidt et al., 2018). Conversely, the Young's modulus of the polystyrene substrates increased slightly. In this case, the alginate likely forms a three-dimensional network on the plastic surface, adding structural reinforcement. This network can limit the mobility of polystyrene chains, resulting in a stiffer material.

Superscript letters (A-B): Within each respective material group, values in the same column not sharing upper case superscript letters indicate statistically significant differences between each other ( $p < 0.05$ ). Values are expressed as mean  $\pm$  standard deviation ( $n = 3$ ). All measurements are performed in triplicate.

**Table 2** Tensile strength (TS), elongation-at-break (EB) and Young's modulus (YM) values for the different material matrices

Matrix		TS (MPa)	EB (%)	YM (MPa)
Parchment paper	Control	44.85 $\pm$ 2.15 <sup>A</sup>	10.37 $\pm$ 1.29 <sup>B</sup>	1771.54 $\pm$ 30.02 <sup>A</sup>
	Without phages	42.23 $\pm$ 1.82 <sup>A</sup>	12.29 $\pm$ 0.41 <sup>A</sup>	543.93 $\pm$ 82.52 <sup>B</sup>
	With phages	41.21 $\pm$ 1.43 <sup>A</sup>	12.45 $\pm$ 0.65 <sup>A</sup>	564.13 $\pm$ 101.14 <sup>B</sup>
Polystyrene	Control	39.02 $\pm$ 7.62 <sup>A</sup>	3.32 $\pm$ 0.23 <sup>A</sup>	1946.59 $\pm$ 17.59 <sup>A</sup>
	Without phages	42.23 $\pm$ 1.82 <sup>B</sup>	12.29 $\pm$ 0.41 <sup>B</sup>	543.93 $\pm$ 82.52 <sup>A</sup>
	With phages	40.56 $\pm$ 1.46 <sup>AB</sup>	2.88 $\pm$ 0.21 <sup>B</sup>	2334.06 $\pm$ 160.61 <sup>B</sup>

## Fourier Transform Infrared Spectroscopy (FTIR)

FTIR spectroscopy was employed to investigate the chemical composition and surface characteristics of the sodium alginate-based films and coatings. The infrared spectra, presented in Fig. 6A–C, highlight the key functional groups characteristic of sodium alginate, with the main absorption bands marked in red and blue. These include broad bands between 3200 and 3600  $\text{cm}^{-1}$ , attributed to hydroxyl (–OH) stretching vibrations, and prominent bands between 1400 and 16,000  $\text{cm}^{-1}$ , corresponding to asymmetric and symmetric stretching of carboxylate (–COO<sup>−</sup>) groups. Additionally, a distinct peak near 1011  $\text{cm}^{-1}$  is associated with C–O stretching vibrations within the saccharide rings of the alginate structure.

These spectral features are consistent with previous studies, such as Marangoni Júnior et al. (2021), who reported similar absorption peaks at approximately 3344  $\text{cm}^{-1}$  (–OH stretching), 2925  $\text{cm}^{-1}$  (aliphatic C–H stretching), 1040  $\text{cm}^{-1}$  (C–O stretching), and carboxylate-related peaks at 1606  $\text{cm}^{-1}$  (asymmetric COO<sup>−</sup>) and 1406  $\text{cm}^{-1}$  (symmetric COO<sup>−</sup>). In samples containing low concentrations of phage or protein-based additives, a weak amide band was observed near 1548  $\text{cm}^{-1}$ , likely due to overlapping with carbonyl (C=O) stretching signals, resulting in diminished intensity.

The presence of these characteristic alginate peaks on both coated paper and plastic substrates confirms the

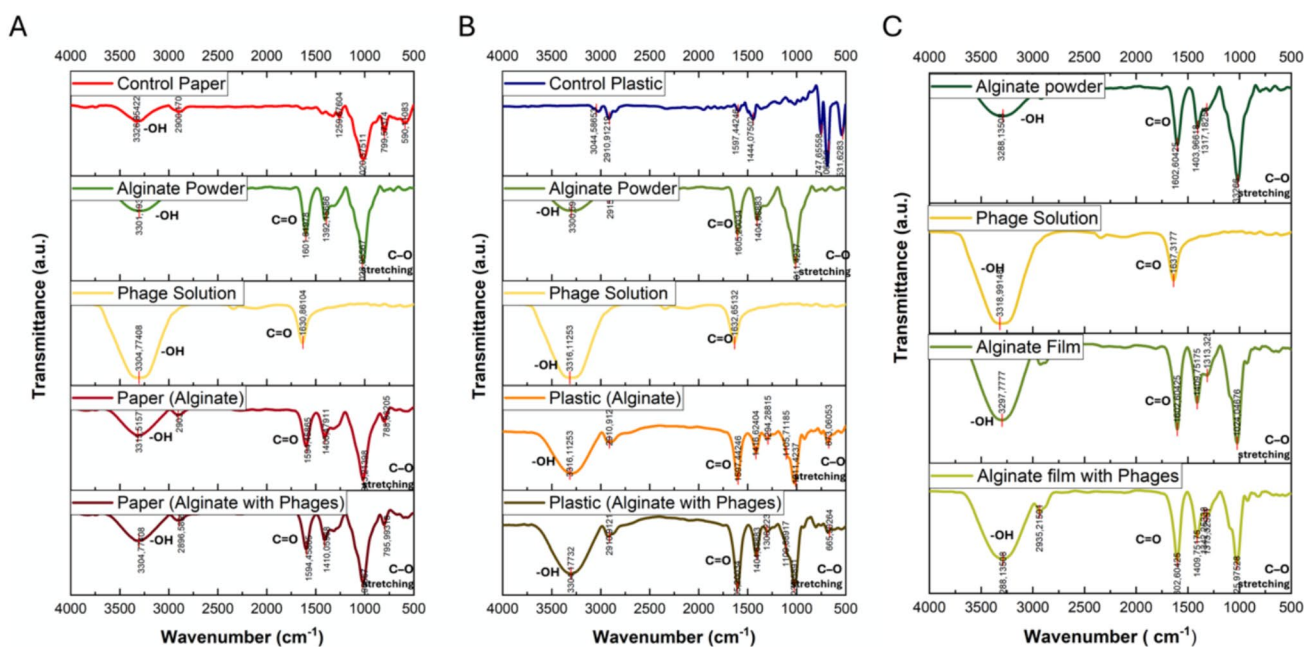
successful deposition of the polymer layer. Importantly, the spectral similarity between the alginate powder, film, and coatings indicates that the coating process did not induce significant chemical modifications in the alginate structure. This chemical stability is essential for preserving the functional properties of the biopolymer, such as its film-forming capacity, biocompatibility, and interaction with other active agents (e.g., antimicrobials or phages).

In addition, the reproducibility of the FTIR signals across different substrates (Fig. 6A–C) demonstrates uniform adhesion and integration of the alginate layer regardless of the substrate type. This suggests strong physical interaction, likely via hydrogen bonding or electrostatic attraction, rather than covalent modification, which is advantageous when substrate recyclability or food safety is a concern.

## Phage Stability

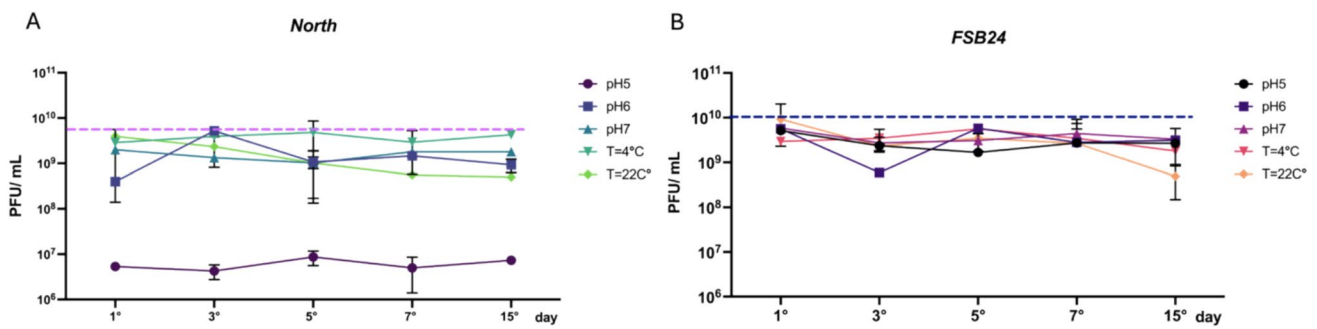
The viability and effectiveness of phages are influenced by environmental factors such as UV radiation, pH, temperature, and salt concentration, with inactivation levels depending on the intensity of these factors and varying across different phage types (Bumunang et al., 2023).

Figure 7 demonstrates the stability of the *E. coli* and *P. fluorescens* phages under various conditions. Panel A shows *E. coli* phages, while Panel B illustrates *P. fluorescens* phages. *E. coli* and *P. fluorescens* phages displayed high stability at 4



**Fig. 6** FTIR spectra comparing control substrates (plastic and paper), alginate powder, phage solution, and alginate-based coatings on different substrates: **A** Coatings on paper, **B** coatings on plastic, and **C** alginate films. Key characteristic peaks of alginate are demonstrated,

including the carboxylate groups (–COO) at 1400–1600  $\text{cm}^{-1}$  and the peak near 1011  $\text{cm}^{-1}$ , corresponding to the C–O stretching vibrations of the saccharide structure



**Fig. 7** Stability of phages over 15 days, maintained at different pH levels (5, 6, and 7) and temperatures (4 °C and 22 °C). **A** *E. coli* phages. **B** *P. fluorescens* phages

°C, maintaining PFU/ml counts throughout the 15-day analysis. However, at room temperature, both types experienced a 1-log reduction over the same period, highlighting cold storage's effectiveness in preserving phage viability, while room temperature storage results in a gradual decline.

Regarding pH tolerance, *P. fluorescens* phages remained stable between pH 5 and 7. However, *E. coli* phages experienced a notable 4-log reduction in viability at pH 5, indicating a pronounced sensitivity to acidic conditions. This observed instability is particularly relevant, as many food products—such as certain fruits, fermented vegetables, and cheeses—have pH values close to 5. Such environments could compromise phage efficacy if not properly addressed.

Nevertheless, this limitation can be overcome by incorporating phages into protective delivery systems, such as polymeric films or edible coatings, which may buffer environmental stress and stabilize phage particles. Additionally, strategies like encapsulation or the inclusion of pH-modulating agents can further enhance phage survival in acidic food matrices. The phage-based coatings developed in this study may be particularly suitable for application on products with pH above 6, such as fresh-cut vegetables, soft cheeses, and minimally processed meats, which are frequently discarded due to contamination by *Pseudomonas fluorescens* and *Escherichia coli*, both of which are common spoilage or pathogenic organisms in such matrices (García-Anaya et al., 2023).

These findings emphasize the importance of tailoring phage delivery systems to the specific conditions of the intended application. Moreover, considering the influence of factors such as genetic variability, geographical origin, and methodology on phage behavior (Bumunang et al., 2023), both in vitro and in situ evaluations are essential to select the most appropriate phage candidates for practical use.

### Load Efficiency and Coating Stability

The efficiency of phage incorporation into the antimicrobial systems varied between films and coatings. As shown

in Fig. 8A, higher incorporation levels were consistently achieved in alginate-based films compared to coatings applied onto paper or polystyrene substrates. In both cases, the incorporated concentrations reached approximately  $10^6$  PFU/mL for *E. coli* and *P. fluorescens* phages, suggesting good initial loading capacity across all tested formats.

Phage stability over time is a critical parameter for the successful application of antibacterial packaging. Previous studies have shown that while the entrapment of phages in polymeric matrices can provide a protective barrier against environmental stressors, it may also contribute to their inactivation due to restricted diffusion, local physicochemical conditions, or interactions with the matrix (García-Anaya et al., 2023).

In this study, the viability of phages embedded in films and coatings was monitored over a 15-day period. Despite some variability in initial incorporation, both phages remained viable during this timeframe. After 15 days, a consistent reduction of approximately 1 log PFU/mL was observed across all materials (Fig. 8B and C), indicating moderate degradation or loss of infectivity.

Remarkably, phage activity was still detectable even after 60 days of storage at room temperature, as evidenced by the inhibition halos observed in agar overlay assays (Fig. 8D). This long-term stability suggests that, despite a gradual loss in titer, the coatings retain antimicrobial potential over extended periods, which is promising for real-world applications in food preservation.

These findings are consistent with previous reports, although the literature presents mixed outcomes regarding phage stability in films. For instance, Gouvêa et al. (2015) reported complete inactivation of a six-phage cocktail incorporated into acetate films within two weeks. This rapid decline was attributed to the lack of direct contact between the film and host bacteria, which limited phage activation. Other studies suggest that phage inactivation may result from shear stress during processing, entrapment within dense polymer matrices, acidity, or antiviral effects of specific biopolymers (García-Anaya et al., 2023).

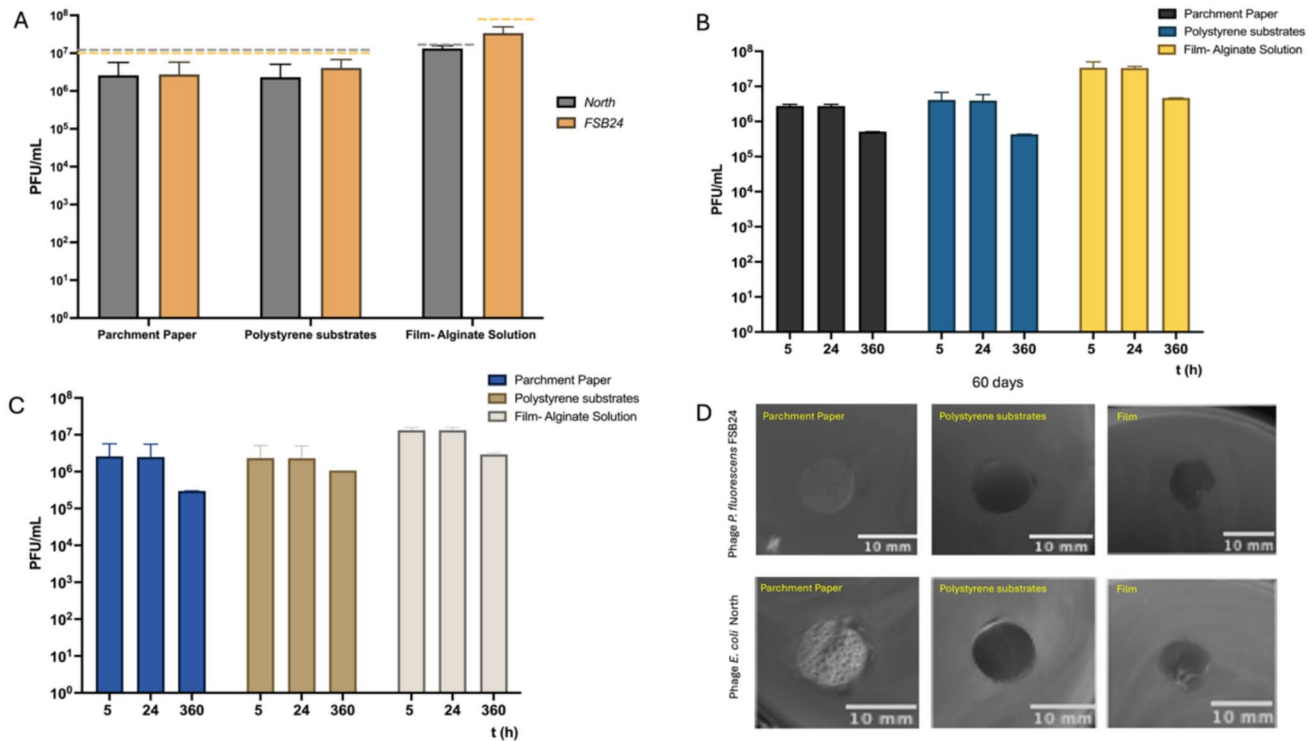


**Fig. 8** Phage incorporation and phage stability on different coating materials over time **(A)** presents the incorporation profile of phages into the samples, comparing *E. coli* and *P. fluorescens* phages across different substrates. **B** Stability of *E. coli* phages on various coatings.

**C** Stability of *P. fluorescens* phages on various coatings. **D** Inhibition halos formed by phage-treated parchment paper, polystyrene substrates, and films after 60 days of incubation

While the exact mechanisms leading to phage decay in biopolymer systems remain unclear, the results of the present study highlight the potential of alginate-based coatings and films to serve as viable carriers for bacteriophages, maintaining infectivity over a practical timeframe. Future work should explore strategies to further enhance phage retention, such as optimizing matrix composition, incorporating protective agents, or using encapsulation techniques.

### Antimicrobial Activity of the Phage-Coated Substrates and Films

The antibacterial activity of the samples was evaluated according to the ISO 22196 standard (International Organization for Standardization [ISO], 2011), which defines the antibacterial activity index (A) as the difference in logarithmic bacterial counts between treated and untreated surfaces after 24 h. According to this standard,  $A < 2$  indicates low antibacterial efficacy,  $2 \leq A < 3$  indicates significant efficacy, and  $A \geq 3$  indicates strong antibacterial efficacy. The samples exhibited significant and strong antibacterial activity against *P. fluorescens* in film samples and on coated substrates (Table 3). The observed differences in antimicrobial activity may be related to the concentration

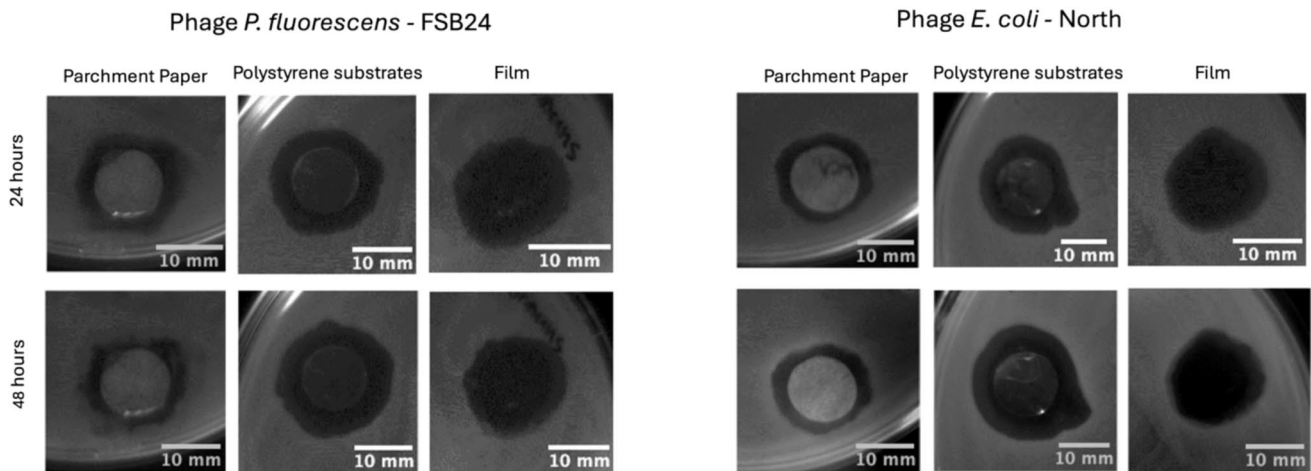
of phages present in each delivery format. In the coatings applied by ultrasonic spray, the phages are confined to a thin surface layer with an estimated thickness of approximately 11  $\mu\text{m}$ . In contrast, in the cast films, the phages are dispersed throughout a thicker matrix, around 30  $\mu\text{m}$ , which may lead to a lower effective surface concentration. Despite this, the samples showed limited antibacterial activity against *E. coli*, with only a 1-log reduction in bacterial count after 24 h.

The antimicrobial activity of the coatings and films developed in this study was evidenced by the formation of clear inhibition halos on culture plates after overnight incubation at 30 °C and 37 °C, confirming the lytic action of the phages against *E. coli* and *P. fluorescens*. The diameter of the halos was measured as an indicator of phage diffusion and efficacy in each material tested. Figure 9 shows the inhibition halos formed on the culture plates, illustrating the antimicrobial effect of the phage-containing coatings and films.

These findings are in line with previous studies demonstrating the potential of bacteriophage-loaded materials for food safety applications. For example, Amarillas et al. (2018) investigated chitosan-based edible coatings incorporating phage vB\_EcoMH2W against *E. coli* O157 on tomato surfaces. Phage-treated tomatoes showed a 3-log reduction

**Table 3** Antibacterial efficacy of sodium alginate-based films and coatings incorporated with *P. fluorescens* and *E. coli* phages, including log reduction values and inhibition halo diameters (mm) observed after 24 and 48 h of incubation

Phage	Matrix	Antibacterial activity (A)	Efficacy of antibacterial property	Halo diameters (mm)	
				24 h	48 h
<i>FSB24</i>	Parchment Paper	4.87	Strong	16 ± 0.6	18 ± 0.6
	Polystyrene substrates	4.90	Strong	20 ± 0.6	20 ± 0.6
	Film	2.95	Significant	15 ± 0.6	17 ± 0.7
<i>North</i>	Parchment Paper	0.05	Low	17 ± 0.6	17 ± 0.6
	Polystyrene substrates	0.85	Low	20 ± 0.6	21 ± 0.6
	Film	0.19	Low	15 ± 0.7	17 ± 0.7

**Fig. 9** Antimicrobial activity of phage-incorporated sodium alginate-based films and coatings against *P. fluorescens* and *E. coli*. Images show inhibition halos formed by phage-treated films, parchment paper, and polystyrene substrates after 24 and 48 h of incubation

in bacterial load after 6 days at 20 °C, compared to untreated controls, highlighting the sustained efficacy of phages embedded in biopolymer matrices under storage conditions.

Similarly, Alves et al. (2019) used calcium chloride cross-linked sodium alginate films to encapsulate phage  $\phi$ IBB-PF7A and tested its performance against *P. fluorescens* on poultry meat. The films preserved phage viability for up to 8 weeks under refrigeration and achieved a 2-log reduction in bacterial counts within the first 2 days, which was maintained through day five.

In the present study, phage-loaded parchment paper, polystyrene coatings, and alginate films continued to exhibit antimicrobial activity after 60 days of storage, as demonstrated qualitatively by inhibition halos (Fig. 8D). These results are particularly relevant as they suggest not only short-term efficacy, as observed in the 24-h ISO 22196-based tests (Table 3), but also long-term stability of phage activity in the packaging materials under ambient conditions.

However, the reduced antibacterial activity against *E. coli* observed in Table 3 may be explained, at least in part, by the larger size of *E. coli* phages, which could hinder

their diffusion through the polymer matrix. Limited mobility may reduce the number of active viral particles reaching the material surface during the initial phases of contact with the target bacteria, especially in dense or cross-linked polymer networks (Hu et al., 2010).

Taken together, these findings reinforce the feasibility of using phage-functionalized coatings and films as antimicrobial strategies in food packaging. They also highlight the importance of considering phage morphology, matrix composition, and application context to optimize the delivery and activity of embedded bacteriophages.

Values are expressed as mean ± standard deviation ( $n = 3$ ). All measurements are performed in triplicate.

## Conclusions

The incorporation of phages into food packaging has shown promise as an effective natural antimicrobial solution for the food industry. Understanding the specific parameters of delivery systems — such as exposure temperature, pH, food product type, pathogen type, and specific bacterial strains

— can facilitate the development of new materials with high antimicrobial application.

In this study, the stability and antimicrobial activity of phages, *P. fluorescens* phage (FSB24) and *E. coli* phage (North), in sodium alginate solutions applied as films and coatings, suggest the potential of these materials for use in food packaging. Such coatings could be especially valuable for items like cheese, meat, vegetables, and fruits that are at risk of contamination from these pathogens and have limited shelf life. This approach could ensure both phage stability and effective antimicrobial action, thereby enhancing food safety and extending the freshness of these products.

**Supplementary Information** The online version contains supplementary material available at <https://doi.org/10.1007/s11947-025-03996-2>.

**Acknowledgements** Sanna Sillankorva acknowledges funding by FCT through the individual scientific employment program contract (2020.03171.CEECIND)

**Author Contributions** Fernanda Coelho: Writing – review & editing, Methodology, Investigation. Victor Gomes Lauriano de Souza: Writing – review & editing, Methodology, Investigation. Lorenzo Pastrana: Supervision, Resources, Funding acquisition. Sanna Sillankorva: Supervision, Writing – review & editing, Methodology, Investigation. Valtencir Zucolloto: Supervision, Resources, Funding acquisition.

Lorenzo Pastrana: Supervision, Resources, Funding acquisition. Sanna Sillankorva: Supervision, Writing – review & editing, Methodology, Investigation. Valtencir Zucolloto: Supervision, Resources, Funding acquisition.

**Funding** The authors acknowledge final support from the FAPESP (Grant N°. 2023/14222–7).

Fundação de Amparo à Pesquisa do Estado de São Paulo, 2023/14222-7

**Data Availability** No datasets were generated or analysed during the current study.

## Declarations

**Competing interests** The authors declare no competing interests.

## References

- Adams, M. H. (1959). Bacteriophages. *Interscience Publishers*. <https://doi.org/10.1002/ange.19620740437>
- Alves, D., Marques, A., Milho, C., Costa, M. J., Pastrana, L. M., Cerqueira, M. A., et al. (2019). Bacteriophage  $\phi$ IBB-PF7A loaded on sodium alginate-based films to prevent microbial meat spoilage. *Int J Food Microbiol*, 291, 121–127. <https://doi.org/10.1016/j.ijfoodmicro.2018.11.026>
- Alves, L. C., Cerqueira, M. A., Gonzalez-Gomez, M. A., Garcia-Acedo, P., Prieto, A. A., Redondo, Y. P., Pastrana, L., & Rivas, J. (2024). Innovative films by embedding magnetic nanoparticles in cellulose acetate. *Food Packaging and Shelf Life*, 42, 101264. <https://doi.org/10.1016/J.FPSL.2024.101264>
- Amarillas, L., Lightbourn-Rojas, L., Angulo-Gaxiola, A. K., Basilio Heredia, J., González-Robles, A., & León-Félix, J. (2018). The antibacterial effect of chitosan-based edible coating incorporated with a lytic bacteriophage against *Escherichia coli* O157: H7 on the surface of tomatoes. *Journal of Food Safety*, 38, Article e12571. <https://doi.org/10.1111/jfs.12571>
- American Society for Testing and Materials (ASTM). (2007). *ASTM D646-96: Standard test method for grammage of paper and paper-board (mass per unit area)*. ASTM International. <https://www.astm.org/d0646-96.html>
- American Society for Testing and Materials (ASTM). (2010). *ASTM D882-10: Standard test method for tensile properties of thin plastic sheeting*. ASTM International. <https://www.astm.org/d0882-10.html>
- American Society for Testing and Materials (ASTM). (2013). *ASTM E96/E96M-13: Standard test methods for water vapor transmission of materials*. ASTM International. <https://www.astm.org/e0096-13.html>
- Anvar, A. A., Ahari, H., & Ataee, M. (2021). Antimicrobial properties of food nanopackaging: A new focus on foodborne pathogens. *Frontiers in Microbiology*. <https://doi.org/10.3389/fmicb.2021.690706>
- Bumunang, E. W., Zaheer, R., Niu, D., Narvaez-Bravo, C., Alexander, T., McAllister, T. A., & Stanford, K. (2023). Bacteriophages for the targeted control of foodborne pathogens. *Foods*, 12, Article Article 2734. <https://doi.org/10.3390/foods12142734>
- Costa, M. J., Marques, A. M., Pastrana, L. M., Teixeira, J. A., Sillankorva, S. M., & Cerqueira, M. A. (2018). Physicochemical properties of alginate-based films: Effect of ionic crosslinking and mannuronic and guluronic acid ratio. *Food Hydrocolloids*, 81, 442–448. <https://doi.org/10.1016/j.foodhyd.2018.03.014>
- Costa, M. J., Pastrana, L. M., Teixeira, J. A., Sillankorva, S. M., & Cerqueira, M. A. (2023). Bacteriophage delivery systems for food applications: Opportunities and perspectives. *Viruses*, 15, Article 1271. <https://doi.org/10.3390/v15061271>
- Darling, A. E., Mau, B., & Pema, N. T. (2010). Progressive Mauve: Multiple genome alignment with gene gain, loss and rearrangement. *PLoS ONE*, 5, 6. <https://doi.org/10.1371/journal.pone.0011147>
- Espitia, P. J. P., Avena-Bustillos, R. J., Du, W. X., Teófilo, R. F., Soares, N. F., & McHugh, T. H. (2014). Optimal antimicrobial formulation and physical-mechanical properties of edible films based on açai and pectin for food preservation. *Food Packaging and Shelf Life*, 2, 38–49. <https://doi.org/10.1016/j.fpsl.2014.06.002>
- Feng, W., Wu, W., Zhao, Z., Gomez, J. Y., Orme, C. J., Tang, W., Bian, W., Priest, C., Stewart, F. F., Jin, C., & Ding, D. (2023). Mathematical model-assisted ultrasonic spray coating for scalable production of large-sized solid oxide electrochemical cells. *ACS Applied Materials & Interfaces*, 15(26), 31430–31437.
- García-Anaya, M. C., Sepulveda, D. R., Zamudio-Flores, P. B., & Acosta-Muniz, C. H. (2023). Bacteriophages as additives in edible films and coatings. *Trends in Food Science & Technology*, 132, 150–161. <https://doi.org/10.1016/j.tifs.2023.01.008>
- Gonzalez-Menendez, E., Fernandez, L., Gutierrez, D., Rodríguez, A., Martínez, B., & García, P. (2018). Comparative analysis of different preservation techniques for the storage of *Staphylococcus* phages aimed for the industrial development of phage-based antimicrobial products. *PLoS ONE*, 13, Article e0205728. <https://doi.org/10.1371/journal.pone.0205728>
- Gouvêa, D. M., Mendonça, R. C. S., Soto, M. L., & Cruz, R. S. (2015). Acetate cellulose film with bacteriophages for potential antimicrobial use in food packaging. *LWT - Food Science and Technology*, 63, 85–91. <https://doi.org/10.1016/j.lwt.2015.03.014>
- Grant, J.R., Enns, E., Marinier, E., Mandal, A., Herman, E.K., Chen, C., Graham, M., Domselaar, G.V., Stothard, P. (2023) Proksee: In-depth characterization and visualization of bacterial genomes. *Nucleic Acids Research*, 51. <https://doi.org/10.1093/nar/gkad326>
- Hu, J., Miyanaga, K., & Tanji, Y. (2010). Diffusion properties of bacteriophages through agarose gel membrane. *Biotechnology Progress*, 26(5), 1213–1221. <https://doi.org/10.1002/btpr.447>

- International Organization for Standardization (ISO). (2011). *ISO 22196:2011 Measurement of antibacterial activity on plastics and other non-porous surfaces*. Geneva, ISO.
- Johno, D., Zhang, Y., Mohammadi, T. N., Zhao, J., Lin, Y., Wang, C., Lu, Y., Abdelaziz, M. N. S., Maung, A. T., Lin, C. Y., El-Telbany, M., Lwin, S. Z. C., Damaso, C. H., Masuda, Y., Honjoh, K., & Miyamoto, T. (2024). Characterization of selected phages for biocontrol of food-spoilage pseudomonads. *Int Microbiol*, *27*, 1333–1344. <https://doi.org/10.1016/j.crf.2021.02.001>
- Jost, V., Kobsik, K., Schmid, M., & Noller, K. (2014). Influence of plasticiser on the barrier, mechanical and grease resistance properties of alginate cast films. *Carbohydrate Polymers*, *110*, 309–319. <https://doi.org/10.1016/j.carbpol.2014.03.096>
- Kopacic, S., Walzl, A., Zankel, A., Leitner, E., & Bauer, W. (2018). Alginate and chitosan as a functional barrier for paper-based packaging materials. *Coatings*, *8*, Article 235. <https://doi.org/10.3390/coatings8070235>
- Lefort, V., Desper, R., & Gascuel, O. (2015). FastME 2.0: A comprehensive, accurate, and fast distance-based phylogeny inference program. *Mol Biol Evol*, *32*(10), 2798–2800. <https://doi.org/10.1093/molbev/msv150>
- Li, X., Tabil, L. G., & Panigrahi, S. (2007). Chemical treatments of natural fiber for use in natural fiber-reinforced composites: A review. *Journal of Polymers and the Environment*, *15*, 25–33. <https://doi.org/10.1007/s10924-006-0042-3>
- Marangoni Júnior, L., Rodrigues, P. R., Silva, R. G., Vieira, R. P., & Alves, R. M. V. (2021). Sustainable packaging films composed of sodium alginate and hydrolyzed collagen: Preparation and characterization. *Food Bioprocess Technology*, *14*, 2336–2346. <https://doi.org/10.1007/s11947-021-02727-7>
- Meier-Kolthoff, J. P., Auch, A. F., Klenk, H. P., & Goker, M. (2013). Genome sequence-based species delimitation with confidence intervals and improved distance functions. *BMC Bioinformatics*, *14*, Article Article 60. <https://doi.org/10.1186/1471-2105-14-60>
- Meier-Kolthoff, J. P., & Goker, M. (2017). VICTOR: Genome-based phylogeny and classification of prokaryotic viruses. *Bioinformatics*, *33*(21), 3396–3404. <https://doi.org/10.1093/bioinformatics/btx440>
- Pajunen, M., Kiljunen, S., & Skurnik, M. (2000). Bacteriophage phi YeO3-12, specific for *Yersinia enterocolitica* serotype O : 3, is related to coliphages T3 and T7. *Journal of Bacteriology*, *182*, 5114–5120. <https://doi.org/10.1128/JB.182.18.5114-5120.2000>
- Pandey, S., Sharma, K., & Gundabala, V. (2022). Antimicrobial bio-inspired active packaging materials for shelf life and safety development: A review. *Food Bioscience*, *48*, Article 101730. <https://doi.org/10.1016/j.fbio.2022.101730>
- Parreidt, T. S., Muller, K., & Schmid, M. (2018). Alginate-based edible films and coatings for food packaging applications. *Foods*, *7*, Article 170. <https://doi.org/10.3390/foods7100170>
- Petraru, A., & Amariei, S. (2023). A novel approach about edible packaging materials based on oilcakes-A review. *Polymers*, *15*(16), Article 3431. <https://doi.org/10.3390/polym15163431>
- Sambrook, J., & Russell, D. W. (2001). *Molecular cloning a laboratory manual* (3rd ed., Vol 1.). Cold Spring Harbor Laboratory Press.
- Soni, K. A., Nannapaneni, R., & Hagens, S. (2016). Reduction of *Listeria monocytogenes* on the surface of fresh-cut cantaloupe and lettuce by bacteriophage application. *Food Microbiology*, *57*, 41–46.
- Tanpichai, S., Srimarut, Y., Woraprayote, W., & Malila, Y. (2022). Chitosan coating for the preparation of multilayer coated paper for food-contact packaging: Wettability, mechanical properties, and overall migration. *International Journal of Biological Macromolecules*, *213*, 534–545. <https://doi.org/10.1016/j.ijbiomac.2022.05.193>
- Technical Association of the Pulp and Paper Industry - Tappi 441 om-98. (2004). *Water absorptiveness of sized (non-bibulous) paper, paperboard, and corrugated fiberboard (Cobb test)*. Norcross: Tappi Press.
- Viazis, S., Akhtar, M., Feirtag, J., & Diez-Gonzalez, F. (2011). Reduction of *Escherichia coli* O157: H7 viability on leafy green vegetables by treatment with a bacteriophage mixture and trans-cinnamaldehyde. *Food Microbiology*, *28*(1), 149–157.
- Wang, D., Lian, F., Yao, S., Liu, Y., Wang, J., Song, X., et al. (2020). Simultaneous detection of three foodborne pathogens based on immunomagnetic nanoparticles and fluorescent quantum dots. *ACS Omega*, *5*, 23070–23080. <https://doi.org/10.1021/acsomega.0c02833>
- World Health Organization. (2024). *Foodborne diseases*. Available online: [https://www.who.int/health-topics/foodborne-diseases#tab=tab\\_1](https://www.who.int/health-topics/foodborne-diseases#tab=tab_1). Accessed 13 Nov 2024.
- Yang, Y., Du, H., Zou, G., Song, Z., Zhou, Y., Li, H., Tan, C., Chen, H., Fischetti, V. A., & Li, J. (2023). Encapsulation and delivery of phage as a novel method for gut flora manipulation *in situ*: A review. *Journal of Controlled Release*, *353*, 634–649. <https://doi.org/10.1016/j.jconrel.2022.11.048>

**Publisher's Note** Springer Nature remains neutral with regard to jurisdictional claims in published maps and institutional affiliations.

Springer Nature or its licensor (e.g. a society or other partner) holds exclusive rights to this article under a publishing agreement with the author(s) or other rightsholder(s); author self-archiving of the accepted manuscript version of this article is solely governed by the terms of such publishing agreement and applicable law.